Ubiquitination regulates granulostasis and DRiP accumulation in SGs under heat stress via the E3 ligase MKRN2

Emmanuel Amzallag1,2, Yehuda M. Danino1,2, Valentina Secco 3, Serena Carra 3, Eran Hornstein1,2#

1Department of Molecular Genetics, Weizmann Institute of Science, Israel.

2Department of Molecular Neuroscience, Weizmann Institute of Science, Israel.

3 Department of Biomedical, Metabolic and Neural Sciences, University of Modena and Reggio Emilia Modena, Italy.

Corresponding Author: Eran.Hornstein@weizmann.ac.il

Abstract

Stress granules (SGs) are transient cytoplasmic biomolecular condensates that play a role in the cellular response to proteotoxic stress. It has been previously shown that ubiquitination regulates SG dynamics; however, the specific mechanisms by which ubiquitin affects SGs are not fully understood. Here, using proximity proteomics, we discover that the engagement of several E3 ubiquitin ligases in SGs is dependent on UBA1 activity. A detailed study of the E3 ubiquitin-protein ligase Makorin 2 (MKRN2) demonstrated that it is localized to SGs in a manner dependent on active ubiquitination. MKRN2 promotes both the proper formation of SGs and their disassembly following stress recovery, by preventing the accumulation of defective ribosomal products (DRiPs) within SGs. Therefore, MKRN2 is a novel regulator of SGs that mediates the maintenance of granulostasis, suggesting that the localization of a subset of E3 ligases into SGs is linked to their capacity to ubiquitinate target proteins.

24 **Introduction**

25 Stress granules (SGs) are biomolecular condensates that form via a process of liquid-liquid phase
26 separation (LLPS) of biomacromolecules (1). SG assembly is initiated by a variety of stressors,
27 including heat stress, oxidative stress, osmotic stress, and ER stress, during which the cell
28 activates the integrated stress response (ISR) (2). Phosphorylation of eIF2α initiates the ISR,
29 resulting in polysome disassembly and global shutdown of translation. This releases mRNA
30 molecules from ribosomes and engages a variety of RNA-binding proteins (RBPs) to form
31 multivalent interactions with both RNA and with other proteins via RNA-binding domains (RBDs)
32 and intrinsically disordered domains (IDD), respectively, resulting in the formation of discrete SGs.
33 Upon recovery from stress, SGs rapidly disassemble, and their dissolution allows mRNAs to be
34 redirected to translation (1).

35 However, SGs can fail to disassemble and persist for longer time, affecting the cells' ability to
36 restore translation, as well as the retro-translocation in the nucleus of RBPs (1). Several factors
37 can delay SG disassembly including the accumulation of misfolded and damaged proteins and
38 the impairment of the protein quality control system. The latter refers to molecular chaperones
39 and protein degradation systems that cooperates to detect unfolded/misfolded proteins and
40 promote their clearance (3). Amongst the misfolded and potentially toxic proteins that can
41 accumulate inside SGs changing their dynamic liquid-like properties are disease-linked mutated
42 RBPs such as TDP-43 or FUS or hnRNPA1 (4–6), as well as defective ribosomal products
43 (DRiPs), which are truncated proteins released from disassembling polyribosomes. DRiPs are
44 rapidly polyubiquitinated for degradation by the ubiquitin-proteasome system as well as by
45 autophagy (7). Amongst the chaperones that participate in the maintenance of SG dynamics are
46 the ATP-dependent chaperone complexes HSP70/HSPB8/BAG3 and VCP/UFD1L/PLAA. These
47 chaperone complexes reduce DRiP accumulation inside SGs (8–10). Accordingly, the activity of

48 HSP70, VCP, and also the autophagic machinery, thus helps surveil stress-induced DRiPs and
49 maintain SGs functioning properly, in a process termed granulostasis (10).

50 Until now, the maintenance of granulostasis under stress has been largely associated with the
51 activity of specific molecular chaperones, namely the HSP70/HSPB8/BAG3 and
52 VCP/UFD1L/PLAA complexes (8,9). The ubiquitin-proteasome system (UPS) is a major
53 component of cellular protein degradation and mediates the conjugation of ubiquitin onto target
54 molecules marked for proteasomal degradation. While ubiquitination and SUMOylation, have
55 been shown to impact SG dynamics as well (11–13) it is unknown if they regulate DRiPs
56 accumulation in SGs.

57 Active ubiquitination is required for proper SG disassembly (11,14–17); however, the specific E3
58 ligases that maintain proper SG dynamics and granulostasis are only partially known. For
59 example, the E3 ligase TRIM21 controls G3BP1 ubiquitination and SG condensation and the E3
60 ligase HECT regulates SG disassembly (16,17). However, whether specific E3 ligases regulate
61 the clearance of DRiPs from SGs has not been yet explored.

62 Here, we report ubiquitination-dependent changes in SG proteomic composition that led to the
63 identification of Makorin 2 (MKRN2) as an important SG-engaged E3 ligase that regulates SG
64 dynamics and the sequestration of stress-induced DRiPs into SGs.

65 **Results**

66 **Ubiquitination affects stress granule dynamics and composition**

67 It was recently shown that active ubiquitination is required for proper SG disassembly
68 (11,14,15,18). However, a detailed characterization of how SGs and the UPS interact has not
69 been achieved. Using G3BP1-mCherry expressing U2OS cells (in which the endogenous G3BP1
70 and 2 genes were knocked out) (19) we studied the full SG assembly and disassembly cycle,
71 induced by heat stress (HS; 43°C followed by stress recovery at 37°C; Fig. 1A,1B). Inhibition of
72 the ubiquitin-activating enzyme UBA1 (ubiquitin-like modifier-activating enzyme 1) by TAK243 (1
73 μM) facilitated SG assembly, while delaying their dissolution (Fig. 1A-C, Supplementary fig. 1).
74 Treatment with TAK243 coupled with HS caused SGs to nucleate and begin assembling earlier
75 than in HS-treated cells (Fig.1B, 1C). SG disassembly following recovery from heat stress, at 37
76 °C, was also delayed (Fig.1A, B, D, Supplementary fig. 1).

77 To determine whether active ubiquitination affects SG liquidity, we performed fluorescence
78 recovery after photobleaching (FRAP) on cells under HS, following UBA1 inhibition. Inhibition of
79 ubiquitination delayed fluorescence recovery dynamics of G3BP1-mCherry, relative to HS treated
80 cells (Figure 1F, Supplementary fig. 6A). These observation indicate that ubiquitination is required
81 for maintaining SG liquidity, consistent with previous reports (14).

82 To characterize the composition of SGs and identify players of the ubiquitination pathway that are
83 involved in maintaining SG dynamics, we used APEX proximity labeling coupled to mass
84 spectrometry (APEX-MS). G3BP1/2 KO U2OS cells expressing G3BP1-APEX were used to label
85 SG proteins, while U2OS cells expressing nuclear export signal (NES)-APEX were used to label
86 the surrounding cytoplasm). Heat stress was induced (43°C; 90 min), UBA1 was inhibited with
87 TAK243, and proximity labeling was induced with biotin phenol (500 μM) and a short hydrogen
88 peroxide pulse (1mM, 60 seconds). Biotin-labelled proteins were isolated with streptavidin
89 magnetic beads and analyzed by mass spectrometry. Samples without biotin-phenol were used

90 to identify and subtract non-APEX-derived biotinylation background. Peptide reads were mapped
91 to proteins with the MaxQuant search engine (v1.6.6.0). Relative to the NES cytoplasmic control,
92 6200 proteins interacting with G3BP1-APEX were identified, including previously-reported SG
93 proteins (Fig. 2A), providing confidence that our protocol effectively isolated SG proteomes. To
94 understand which proteins are associated with SGs in a ubiquitination-dependent manner, we
95 next compared the HS-induced SG proteomes without or with TAK243 (Fig. 2B, Supplementary
96 fig. 2A,B). This provided a list of proteins either enriched (83 proteins) or depleted (215 proteins)
97 from SGs upon inhibition of ubiquitination (Student's T-test, FDR<0.05; Fig. 2C). Amongst the
98 proteins that associated with SGs in a ubiquitin-dependent manner we report HSPA12, DNAJA1,
99 and the VCP cofactors, UFD1L, NSFL1C, FAF1, and PLAA. Interestingly, these chaperones were
100 previously implicated in promoting SG disassembly by preventing aberrant accumulation of
101 stress-damaged proteins (9,14). Ubiquitin hydrolases and E3 ligases were also associated with
102 SGs in a ubiquitination-dependent manner, including the RNA-binding ubiquitin ligases (RBULs)
103 MKRN2, CNOT4, TRIM25, and ZNF598. We orthogonally validated the ubiquitin-dependent
104 interaction of the most SG-depleted E3 ligase, MKRN2, by immunofluorescence in U2OS cells
105 fixed after 90 min HS, without or with TAK243 (Fig. 2D, 2E). In agreement with APEX-MS results,
106 endogenous MKRN2 exhibited decreased SG partitioning in response to TAK243 treatment (Fig.
107 2E).

108 **The E3 ligase MKRN2 affects SG dynamics**

109 While the human genome encodes only 2 E1s and ~30 E2 enzymes, ~600 E3 ligases are known,
110 conferring substrate specificity in targeting specific proteins and cellular pathways (20). To
111 determine whether ubiquitin-sensitive RBULs ligases control SG dynamics, we knocked down
112 CNOT4, ZNF598, and MKRN2 in U2OS cells that were subjected to HS, followed by recovery (43
113 °C, 90 min -> 37 °C). Knockdown of CNOT4, ZNF598, or MKRN2 all impacted SG dynamics to
114 varying degrees (Supplementary Fig. 5A, B). MKRN2 depletion affected both SG assembly and

115 disassembly, with cells forming smaller SGs that took longer to disassemble upon recovery
116 (Figure 3,4). ZNF598 similarly affected SG size but had a smaller impact on disassembly. CNOT4
117 had a minimal effect on SG assembly, with a modest effect on their disassembly (Supplementary
118 Fig. 5A, B). Based on our mass spectrometry data, indicating MKRN2 as the most highly SG-
119 depleted E3 upon TAK243 treatment and its strongest impact on SG dynamics, we focused
120 mechanistic studies on MKRN2.

121 Using SG live imaging, we investigated the consequences of MKRN2 KD on SG dynamics under
122 HS. SG assembly under heat stress typically involves a reduction in SG numbers over time, as
123 smaller condensates coalesce to form larger but fewer SGs (8,21–23). The knockdown (KD) of
124 MKRN2 resulted in a higher number of SGs at 90 min of HS (Fig. 3A, B, D) and the average size
125 of SGs was almost half as small compared to the control (Fig. 3C, El Supplementary fig. 3). These
126 data suggest that SGs fail to coalesce and mature upon MKRN2 KD. Having established that
127 MKRN2 depletion affects SG number and size, we then measured their liquid-like properties by
128 performing FRAP experiments, using the mobility of G3BP1 as readout. Consistently, FRAP
129 analysis demonstrated that MKRN2 KD resulted in a slight increase in SG liquidity (Fig. 3F,
130 Supplementary fig. 6B), that could be interpreted as associated to decreased coalescence into
131 dense and mature SGs (23,24).

132 Then, to further test the impact of MKRN2 on SG dynamics, we overexpressed MKRN2–GFP and
133 we observed that it was recruited to SG (Fig. 3G). We next quantified SG ubiquitin content in
134 response to MKRN2-GFP overexpression, using an antibody that recognizes free, mono- and
135 poly-ubiquitinated proteins (FK2). MKRN2-GFP increased the partitioning of ubiquitin into SGs,
136 relative to neighboring cells that did not express MKRN2-GFP in the same polyclonal mosaic
137 culture (Fig. 3G, 3H). Together these data indicate that MKRN2 regulates the assembly dynamics
138 of SGs by promoting their coalescence during HS and can increase SG ubiquitin content.

139 We next tested the impact of MKRN2 on SG disassembly following stress removal. MKRN2 KD
140 delayed the disassembly of SGs (Fig. 4A, 4B; Supplementary fig. 4). The effect was pronounced
141 30 and 60 minutes after cessation of HS (Fig. 4C, 4D). Therefore, MKRN2 is required for
142 maintaining proper SG dynamics under HS.

143 **MKRN2 regulates accumulation of DRiPs in SGs**

144 DRiPs are truncated peptides that are prone to aggregation and DRiPs ubiquitination affects their
145 solubility and clearance (7,8,25) . Proteostasis impairment causes aberrant DRiP accumulation
146 inside SGs and impairs SG disassembly. This suggests the idea that MKRN2 may ubiquitinate a
147 subset of DRiPs, avoiding their accumulation inside SGs and facilitating their disposal. To test the
148 idea that ubiquitin impacts a subset of DRiPs in SGs, we induced SG formation by HS in absence
149 or presence of the UBA1 inhibitor TAK243. Concomitantly we treated the cells with O-propargyl
150 puromycin (OP-puro, 25uM), which is incorporated into nascent polypeptide chains, causing
151 polysome disassembly and the emergence of DRiPs. We observed increased partitioning of OP-
152 puro labelled DRiPs in SGs upon inhibition of ubiquitination relative to control (Fig. 5A, 5B). These
153 data suggest that active ubiquitination prevents the accumulation of DRiPs inside SGs. To
154 understand whether a fraction of DRiPs is ubiquitinated by MKRN2, we then performed a similar
155 analysis in proficient and MKRN2-deficient cells. We measured increased partitioning of OP-puro
156 labelled DRiPs in SGs upon knockdown of MKRN2, relative to control (Fig. 5C, 5D). Therefore,
157 we conclude that MKRN2 ubiquitinates a subset of DRiPs, avoiding their accumulation inside
158 SGs.

159 Together our study provides evidence for a new role for ubiquitination and for the E3 ligase
160 MKRN2 in the control of SG dynamics and DRiPs turnover.

161

162 **Discussion**

163 In this study, we characterize the impact of ubiquitination on SG proteomic composition during
164 heat stress. Using APEX proximity labeling and mass spectrometry, we demonstrate that
165 ubiquitination regulates SG functions under heat stress by controlling the recruitment of several
166 molecular regulators of proteostasis into SGs.

167 Specifically, ubiquitination regulates the localization of several proteostasis-related proteins to
168 SGs, including four VCP cofactors (UFD1L, PLAA, NSFL1C, and FAF1), two of which (UFD1L
169 and PLAA) have been shown to regulate SG dynamics and sequestration of DRiPs (8). This
170 suggests that ubiquitin-binding VCP cofactors are recruited to SGs through their interaction with
171 ubiquitinated proteins within these condensates. Furthermore, the localization of the heat shock
172 protein HSP70 (HSPA12B) and its co-chaperone DNAJA1 to SGs is also regulated by
173 ubiquitination. This finding is consistent with similar behavior observed under sodium arsenite
174 stress (17) and is likely to influence the accumulation of DRiPs in SGs (9).

175 Several E3 ubiquitin ligases were depleted from SGs in the absence of UBA1 activity, namely
176 MKRN2, ZNF598, CNOT4, TRIM25, and TRIM26, whereas the E3 RNF20 was enriched in SGs.
177 A detailed study of the E3 ligase MKRN2 demonstrated ubiquitination-dependent partitioning of
178 endogenous MKRN2 into SGs. This suggests that the localization of a subset of E3 ligases into
179 SGs is linked to their capacity to ubiquitinate target proteins.

180 Pan et al. reported enrichment of several HECT-domain E3 ligases in SGs following inhibition of
181 ubiquitination by TAK243 (17), suggesting that this process is specific and potentially regulated
182 in a stress- or protein-specific manner. SG E3 ligases that depend on UBA1 activity are RBULs,
183 and their capacity to bind RNA may be particularly intriguing for SG E3s.

184 Endogenous and ectopically expressed MKRN2 were both localized to SGs. MKRN2 has a
185 functional role in regulating SG dynamics under heat stress, and its knockdown results in more

186 numerous and smaller SGs, as well as a significant delay in SG disassembly following recovery
187 from stress.

188 We also show that UBA1 activity and MKRN2 regulates a subset of DRiP homeostasis in SGs.
189 Thus, ubiquitination is required for preventing excessive DRiPs accumulation in SGs under heat
190 stress. We further show that the RBUL MKRN2 similarly prevents accumulation of DRiPs in SGs
191 suggesting that it may execute ubiquitin-mediated extraction of DRiPs from SGs. We note that
192 our experiments cannot delineate whether ubiquitination of DRiPs by MKRN2 occurs inside SGs
193 or in the cytoplasm. However, the finding that MKRN2 is enriched in SGs under stress coupled
194 with the fact that its overexpression increases SG ubiquitin content, suggests that MKRN2
195 controls DRiP clearance from SGs via polyubiquitination of SG-localized substrates. In summary,
196 MKRN2 is the first E3 ligase shown to play a role in DRiP extraction from SGs. The phenotype of
197 smaller, more numerous SGs concomitant with increased DRiP partitioning, also reported upon
198 inhibition of autophagy and VCP function (8), suggests that MKRN2 may act in the same pathway.

199

200 We note that the SG disassembly phenotype upon MKRN2 knockdown is less pronounced than
201 that observed with TAK243 treatment. Therefore, MKRN2 may target a subset of DRiPs.
202 consistent with the role of additional SG-localized E3 ligases, such as ZNF598 or CNOT4, that
203 regulate SG dynamics. Overall, our results support the conclusion that proper SG dynamics
204 depend on clearance of DRiPs from these condensates and portray MKRN2 as a novel
205 proteostasis factor regulating this process.

206 Limitations: The direct MKRN2 substrates and ubiquitin-chain types (K63/K48) are currently
207 unknown. In addition, it is interesting to understand if DRiP solubility is dependent on
208 ubiquitination or on specific E3 ligases, such as MKRN2.

209 In sum, global ubiquitination promotes the recruitment of key SG-engaged chaperones, including
210 HSP70 and VCP, as well as a subset of E3 ubiquitin ligases. We identify the E3 ligase MKRN2
211 as a novel regulator of SG dynamics and proteostatic function. Clearance of DRiPs from SGs
212 requires active ubiquitination and is mediated in part by MKRN2. These insights refine our
213 understanding of how SGs coordinate the triage of stress-damaged proteins with condensate
214 dynamics during proteotoxic stress. Ultimately, defining ubiquitination-dependent regulation of SG
215 composition and function may illuminate new therapeutic avenues for restoring proteostasis in
216 diseases that involve protein aggregation.

217

218 **Methods**

219 **Mammalian cell culture**

220 U2OS cells were cultured in growth media consisting of high glucose DMEM (Sartorius 01-052-
221 1A), 10% FBS (Sigma F7524) and 1% penicillin-streptomycin-amphotericin B (Sartorius 03-033-
222 1B) in a 37°C incubator supplemented with 5% CO_2. To induce heat stress, cells were placed
223 into a dedicated incubator set to 43°C supplemented with 5% CO_2. For UBA1 inhibition, cells
224 were pre-treated with 1uM TAK243 (Med Chem Express; Cat# HY-100487) prior to heat stress.
225 For MKRN2 KD, cells were transfected with MKRN2 siRNA (Dharmacon siGENOME
226 SMARTpool; M-006960-01-0005) using Lipofectamine RNAiMAX (Cat#: 13778075) and
227 cultured for 72 hours before analysis.

228

229 **Molecular cloning**

230 Molecular cloning of MKRN2-GFP was performed using In-Fusion® Snap Assembly (Cat#
231 638947; Takara Clontech) and inserted into pcDNA4.0 vector with puromycin resistance.
232 G3BP1-mCherry cells were transfected with Lipofectamine 2000 (Thermo Fisher Scientific, Cat#
233 11668027) cultured with 5ng/ml puromycin for 7 days.

234

235 **Microscopy**

236 SG live imaging was performed in a Zeiss CD7 widefield microscope equipped with an Axiocam
237 702 CMOS camera using a 20X air objective with an additional 2X post-magnification (effective
238 magnification of 40X, excitation wavelength 590nm). G3BP1-mCherry cells were seeded into
239 optical 24-well plates (Cellvis P24-1.5H-N) and placed into the heated microscope incubator
240 chamber (37°C, 5% CO_2). After one cycle of imaging, the microscope incubator temperature
241 was increased to 43°C. After 90 min of heat stress, the temperature was lowered back down to
242 37°C to image SG disassembly. SG number and area was analysed using the surfaces feature
243 in Imaris software. Immunofluorescent staining was performed on 12mm round glass coverslips

244 inside 24-well plates. Immunofluorescent images were captured in a Zeiss LSM900 confocal
245 microscope using a 63X oil objective lens.
246
247 **FRAP**
248 G3BP1-mCherry cells were seeded into 3.5mm dishes with a central coverslip (MatTek P35GC-
249 1.5-14-C). Cells were imaged in a Leica SP8 STED microscope using a 100X objective. To
250 induce heat stress, the microscope incubator temperature was increased to 43°C and an
251 objective heater was attached to the objective and heated to 43°C. Cells were left in the heated
252 microscope incubator chamber for 60 minutes, and FRAP was performed for 30 minutes
253 thereafter. To photobleach SGs, a 561nm laser set to max power was used to bleach entire
254 SGs. In order to monitor fluorescence recovery, images were collected every 400ms for 63
255 seconds. Fluorescence recovery data was collected using the Leica LasX software. Analysis
256 corrected for background fluorescence intensity and normalized to the pre-bleach SG intensity
257 to calculate the fraction of fluorescence recovery at each time point.
258
259 **APEX proximity labelling**
260 G3BP1-APEX or NES-APEX U2OS (Marmor-Kollet *et al.*) cells were seeded into T125 flasks
261 with 50ng/ml tetracycline (Sigma T7660) and allowed to incubate for 24h before performing
262 APEX experiment. Four technical repeats were used for each condition. Following pre-treatment
263 with TAK243, cells were supplemented with 500uM Biotin-Tyramide (Iris Biotech 41994-02-9)
264 for 90 minutes to allow for labelling activity. Labelling was then induced by addition of H_2O_2 (JT
265 Baker 2186-01) for 60 seconds. APEX activity was extinguished with quenching solution (10mM
266 sodium azide (Sigma cat number S2002), 10mM sodium ascorbate (Alfa Aesar A17759), 5mM
267 Trolox (Sigma 238813) in PBS. Cells were then scraped in PBS, centrifuged at 3000xg for 10
268 minutes at 4°C and the cell pellet was lysed in ice-cold RIPA buffer (50mM Tris-HCl pH8,
269 150mM NaCl, 1% NP-40, 0.5% sodium deoxycholate, 0.1% SDS) supplemented with cOmplete

270 Protease Inhibitor Cocktail (Roche, 4693116001) and PhosSTOP (Roche, 4906837001).
271 Lysates were centrifuged at 15000xg for 10 minutes at 4°C and protein concentration was
272 quantified using Bradford assay (Bio-Rad 5000006). Streptavidin magnetic beads (Thermo
273 Fisher cat number 88817) were incubated with the protein extracts at a ratio of 100ul beads per
274 500ug protein extract overnight at 4°C with rotation.
275

276 **Liquid chromatography and mass spectrometry**

277 Samples were subjected to on-bead tryptic digestion. The resulting peptides were analysed
278 using nanoflow liquid chromatography (nanoAcquity) coupled to high resolution, high mass
279 accuracy mass spectrometry (Q-Exactive Plus). Each sample was analysed on the instrument
280 separately in a random order in discovery mode. Raw data were processed with MaxQuant
281 v1.6.6.0. The data were searched with the Andromeda search engine against the human
282 proteome database, appended with common lab protein contaminants and the default
283 modifications. Quantification was based on the LFQ method, based on unique/all peptides.
284

285 **Proteomics statistical analysis**

286 ProteinGroups output table from MaxQuant was imported into Perseus for analysis. First,
287 contaminants were removed. Raw intensity values were $\log_2$ transformed and missing values
288 imputed for proteins with at least four valid values using an artificial normal distribution with a
289 downshift of 1.8 standard deviations and a width of 0.3 of the original ratio distribution. To
290 identify proteins non-specifically bound to streptavidin beads, student's t test with FDR <=0.05
291 was used to compare each sample to respective no BP control samples. These non-specific
292 binders were filtered out and proteins were then compared between G3BP1-APEX and NES-
293 APEX baits. LFQ values were $\log_2$ transformed and missing values were imputed for proteins
294 with at least two valid values in at least one group using an artificial normal distribution with a
295 downshift of 1.8 standard deviations and a width of 0.3 of the original ratio distribution. Proteins

296 were then compared between the G3BP1-APEX bait to the NES-APEX bait using student's t
297 test with FDR <=0.05 to determine which proteins were significantly enriched in proximity to
298 G3BP1 compared to NES. G3BP1-APEX values were then normalized by the mean of their
299 corresponding NES-APEX values. The NES-normalized values were then compared between
300 the TAK243 vs DMSO treated samples using student's t test with FDR <=0.05.
301
302 **Statistical analysis**
303 Statistical analysis of live imaging data was done using repeated-measures ANOVA test with
304 contrast analysis in R. Pairwise comparisons were done using Welch's t test in Graphpad Prism.
305 Statistical p values < 0.05 were considered significant.
306
307 **Labeling of nascent peptides with OP-puro and high content imaging-based assay**
308 Cells were grown on polylysine-coated glass coverslip. Newly synthesized proteins were
309 labelled by incubating the cells with 25 mM O-Propargyl-puromycin (OP-puro) for the indicated
310 time points and CuAAC detection of OP-puro labelled DRiPs was performed as previously
311 described, using Alexa Fluor 594 azide (A10270, Life Technologies) (PMID: 22160674). Cells
312 were next processed for immunofluorescence microscopy. Blocking and incubation with primary
313 and secondary antibodies were performed in PBS containing 3% BSA and 0.1% Triton X-100.
314 DRiPs enrichment inside SGs was measured using the Scan^R Analysis software (Olympus).
315 SGs were segmented based on G3BP1 signal using edge detection algorithm. The mean
316 fluorescence intensity of OP-puro labelled DRiPs was detected in each detected SG and was
317 additionally measured in an area surrounding each SG. The relative enrichment of OP-puro
318 labelled DRiPs in individual SGs was calculated as a ratio of mean fluorescence intensity inside
319 the SG divided by mean intensity in the region surrounding the SG, as previously described
320 (PMID: 27570075).
321

340 **Contributions statement**

341 E.H. and E.A. oversaw the conceptualization of this study. E.A. and Y.M.D. performed the APEX
342 proteomics experiment. Mass spectrometry was performed at the de Botton Institute for Protein
343 Profiling from the Nancy and Stephen Grand Israel National Center for Personalized Medicine (G-
344 INCPM). E.H. and E.A. designed the study and had unrestricted access to all data. E.A. performed
345 and analyzed all live imaging experiments. E.A. performed immunofluorescence staining,
346 microscopy and analysis of ubiquitin and MKRN2. E.A. performed all FRAP experiments. V.S.
347 and S.C. performed the O-propargyl puromycin fluorescent staining, microscopy and analysis of
348 DRiP partitioning in stress granules. E.A. and E.H participated in drafting the initial manuscript
349 draft and E.H., E.A. and S.C. reviewed and revised the draft. All authors agreed to submit the
350 manuscript, read and approved the final draft, and take full responsibility for its content, including
351 the accuracy of the data and its statistical analysis.

352 **Acknowledgments**

353 Eran Hornstein is the Mondry Family Professorial Chair and Head of the Nella and Leon Benoziyo
354 Centre for Neurological Diseases and of the Andi and Larry Wolfe Centre for Neuroimmunology
355 and Neuromodulation. The authors thank Dr. Yishai Levin, Dr. Alon Savidor, Corine Katina at the
356 de Botton Institute for Protein Profiling from the Nancy and Stephen Grand Israel National Center
357 for Personalized Medicine (G-INCPM) for performing mass spectrometry. The authors thank
358 Yoseph Addadi, Inna Goliand and Tatiana Smirnova from the de Picciotto Cancer Cell
359 Observatory In memory of Wolfgang and Ruth Lesser of the Moross Integrated Cancer Center in
360 the department of Life Science Core Facilities, Weizmann Institute of Science for help with
361 performing live imaging and FRAP. The authors thank Prof. Itay Koren for his advice on our study.
362 The authors thank CIGS (University of Modena microscopy facility) and Dr. Jonathan Vinet for

363 technical support for confocal microscopy image acquisition and analysis. Special thanks to Iddo
364 Magen, Yahel Cohen and Aviad Siany from the Hornstein Lab for fruitful discussion and advice.

365 **Conflict of interests**

366 The authors declare that they have no conflict of interest.

367 **Funding**

368 Eran Hornstein lab is funded by the Andi and Larry Wolfe Centre for Neuroimmunology and
369 Neuromodulation; the Binational Science Foundation (BSF); Association Française Contre les
370 Myopathies (AFM) grants 24882, 28680; Muscular Dystrophy Association (MDA) grant 1280000;
371 Target ALS; Israel Science Foundation (ISF 3497/21, 424/22); ALS Canada; Minna-James-
372 Heineman Stiftung through, Minerva Foundation, with funding from the Federal German Ministry
373 for Education and Research; Robert Packard Center for ALS Research at Johns Hopkins; McGill
374 University; EU - ERA-Net; Radala Foundation for ALS Research; Additional support generously
375 provided by the Kekst Family Institute for Medical Genetics. Weizmann SABRA - Yeda-Sela -
376 WRC Program, the Estate of Emile Mimran, and The Maurice and Vivienne Wohl Biology
377 Endowment. Nella and Leon Benoziyo Center for Neurological Diseases, Goldhirsh-Yellin
378 Foundation. Dr. Sydney Brenner and friends, Weizmann - Center for Research on
379 Neurodegeneration. Redhill Foundation – Sam and Jean Rothberg Charitable Trust Dr. Dvora
380 and Haim Teitelbaum Endowment Fund and Weizmann – Institute for Artificial Intelligence -
381 Acceleration Grant. Target ALS; Israel Science Foundation (ISF 3497/21, 424/22), CReATe
382 Consortium. Carra lab was supported by the Armenise-Harvard and AirAlzh Foundations (AHA
383 Mid-Career Award 2022), the AriSLA Foundation (SUMOsolvable).

384

385 **References**

386 1. Protter DSW, Parker R. Principles and properties of stress granules. Trends Cell Biol. 2016
387 Sept;26(9):668–79.

388 2. Bond S, Lopez-Lloreda C, Gannon PJ, Akay-Espinoza C, Jordan-Sciutto KL. The integrated
389 stress response and phosphorylated eukaryotic initiation factor 2α in neurodegeneration. J
390 Neuropathol Exp Neurol. 2020 Feb 1;79(2):123–43.

391 3. Hipp MS, Kasturi P, Hartl FU. The proteostasis network and its decline in ageing. Nat Rev
392 Mol Cell Biol. 2019 July;20(7):421–35.

393 4. Gordon D, Dafinca R, Scaber J, Alegre-Abarrategui J, Farrimond L, Scott C, et al. Single-
394 copy expression of an amyotrophic lateral sclerosis-linked TDP-43 mutation (M337V) in
395 BAC transgenic mice leads to altered stress granule dynamics and progressive motor
396 dysfunction. Neurobiol Dis. 2019 Jan;121:148–62.

397 5. Baron DM, Kaushansky LJ, Ward CL, Sama RRK, Chian R-J, Boggio KJ, et al.
398 Amyotrophic lateral sclerosis-linked FUS/TLS alters stress granule assembly and
399 dynamics. Mol Neurodegener. 2013 Aug 31;8(1):30.

400 6. Gui X, Luo F, Li Y, Zhou H, Qin Z, Liu Z, et al. Structural basis for reversible amyloids of
401 hnRNPA1 elucidates their role in stress granule assembly. Nat Commun. 2019 May
402 1;10(1):2006.

403 7. Schubert U, Antón LC, Gibbs J, Norbury CC, Yewdell JW, Bennink JR. Rapid degradation
404 of a large fraction of newly synthesized proteins by proteasomes. Nature. 2000 Apr
405 13;404(6779):770–4.

406 8. Seguin SJ, Morelli FF, Vinet J, Amore D, De Biasi S, Poletti A, et al. Inhibition of autophagy,
407 lysosome and VCP function impairs stress granule assembly. Cell Death Differ. 2014
408 Dec;21(12):1838–51.

409 9. Ganassi M, Mateju D, Bigi I, Mediani L, Poser I, Lee HO, et al. A Surveillance Function of
410 the HSPB8-BAG3-HSP70 Chaperone Complex Ensures Stress Granule Integrity and
411 Dynamism. Mol Cell. 2016 Sept 1;63(5):796–810.

412 10. Alberti S, Mateju D, Mediani L, Carra S. Granulostasis: Protein quality control of RNP
413 granules. Front Mol Neurosci. 2017 Mar 27;10:84.

414 11. Maxwell BA, Gwon Y, Mishra A, Peng J, Nakamura H, Zhang K, et al. Ubiquitination is
415 essential for recovery of cellular activities after heat shock. Science. 2021 June
416 25;372(6549):eabc3593.

417 12. Marmor-Kollet H, Siany A, Kedersha N, Knafo N, Rivkin N, Danino YM, et al.
418 Spatiotemporal Proteomic Analysis of Stress Granule Disassembly Using APEX Reveals
419 Regulation by SUMOylation and Links to ALS Pathogenesis. Mol Cell. 2020 Dec
420 3;80(5):876-891.e6.

421 13. Verde EM, Antoniani F, Mediani L, Secco V, Crotti S, Ferrara MC, et al. SUMO2/3
422 conjugation of TDP-43 protects against aggregation. Sci Adv. 2025 Feb
423 21;11(8):eadq2475.

14. Gwon Y, Maxwell BA, Kolaitis R-M, Zhang P, Kim HJ, Taylor JP. Ubiquitination of G3BP1 mediates stress granule disassembly in a context-specific manner. Science. 2021 June 25;372(6549):eabf6548.

15. Tolay N, Buchberger A. Comparative profiling of stress granule clearance reveals differential contributions of the ubiquitin system. Life Sci Alliance [Internet]. 2021 May;4(5). Available from: http://dx.doi.org/10.26508/lsa.202000927

16. Yang C, Wang Z, Kang Y, Yi Q, Wang T, Bai Y, et al. Stress granule homeostasis is modulated by TRIM21-mediated ubiquitination of G3BP1 and autophagy-dependent elimination of stress granules. Autophagy. 2023 July;19(7):1934–51.

17. Pan CR, Knutson SD, Huth SW, MacMillan DWC. μMap proximity labeling in living cells reveals stress granule disassembly mechanisms. Nat Chem Biol. 2025 Apr;21(4):490–500.

18. Tolay N, Buchberger A. Role of the ubiquitin system in stress granule metabolism. Int J Mol Sci. 2022 Mar 26;23(7):3624.

19. Kedersha N, Panas MD, Achorn CA, Lyons S, Tisdale S, Hickman T, et al. G3BP-Caprin1-USP10 complexes mediate stress granule condensation and associate with 40S subunits. J Cell Biol. 2016 Mar 28;212(7):845–60.

20. Clague MJ, Heride C, Urbé S. The demographics of the ubiquitin system. Trends Cell Biol. 2015 July;25(7):417–26.

21. Chernov KG, Barbet A, Hamon L, Ovchinnikov LP, Curmi PA, Pastré D. Role of microtubules in stress granule assembly. J Biol Chem. 2009 Dec;284(52):36569–80.

22. Hu S, Zhang Y, Yi Q, Yang C, Liu Y, Bai Y. Time-resolved proteomic profiling reveals compositional and functional transitions across the stress granule life cycle. Nat Commun. 2023 Nov 27;14(1):7782.

23. Van Treeck B, Parker R. Principles of stress granules revealed by imaging approaches. Cold Spring Harb Perspect Biol. 2019 Feb 1;11(2):a033068.

24. Wheeler JR, Matheny T, Jain S, Abrisch R, Parker R. Distinct stages in stress granule assembly and disassembly. Elife [Internet]. 2016 Sept 7;5. Available from: http://dx.doi.org/10.7554/elife.18413

25. Qian S-B, Princiotta MF, Bennink JR, Yewdell JW. Characterization of rapidly degraded polypeptides in mammalian cells reveals a novel layer of nascent protein quality control. J Biol Chem. 2006 Jan 6;281(1):392–400.

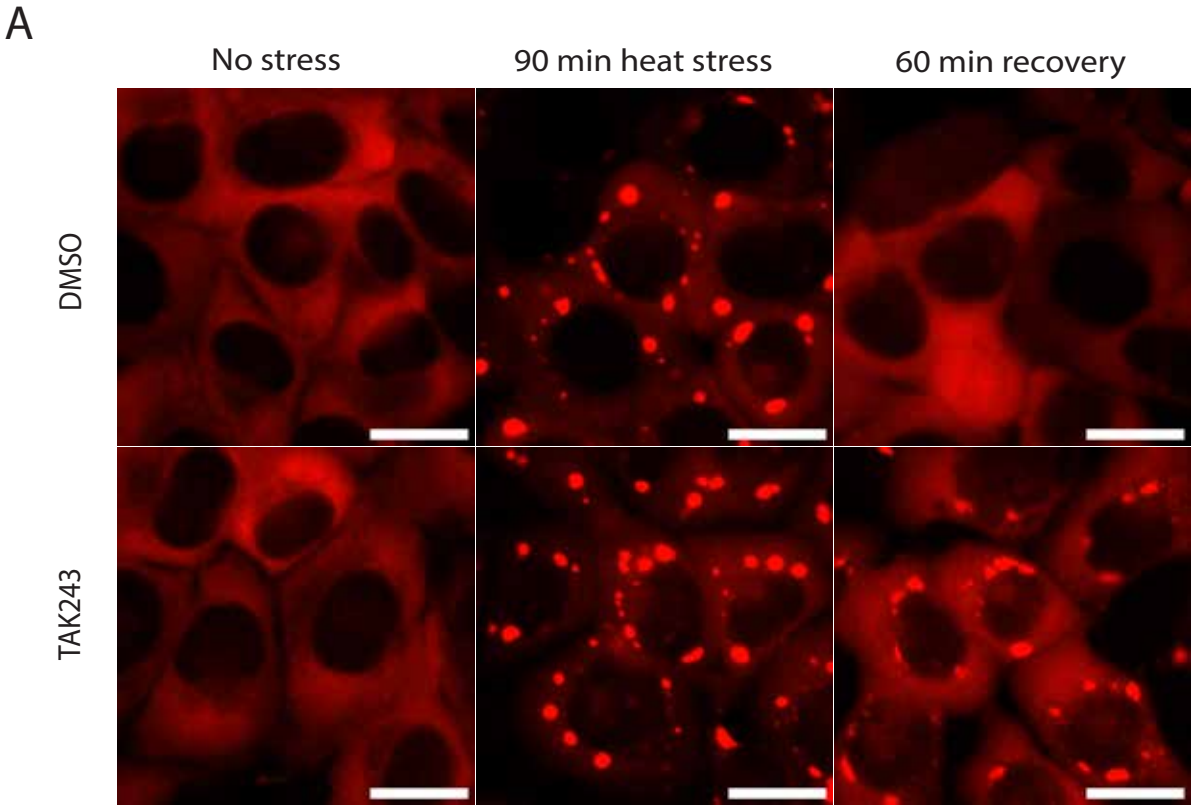
A
No stress
90 min heat stress
60 min recovery
DMSO
TAK243

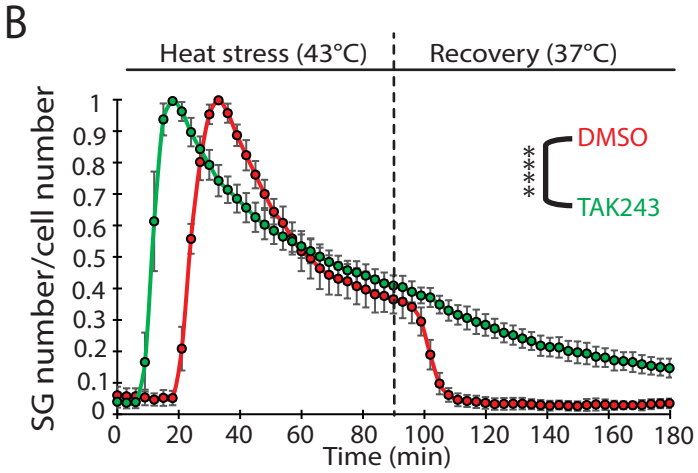
B
Heat stress (43°C)
Recovery (37°C)
SG number/cell number
Time (min)
****
DMSO
TAK243

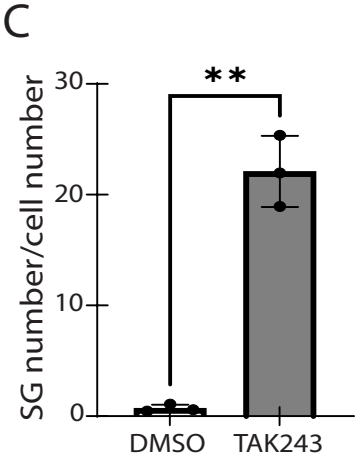
C
SG number/cell number
**
DMSO
TAK243

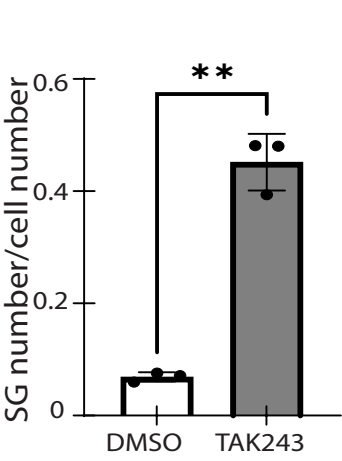
D
SG number/cell number
**
DMSO
TAK243

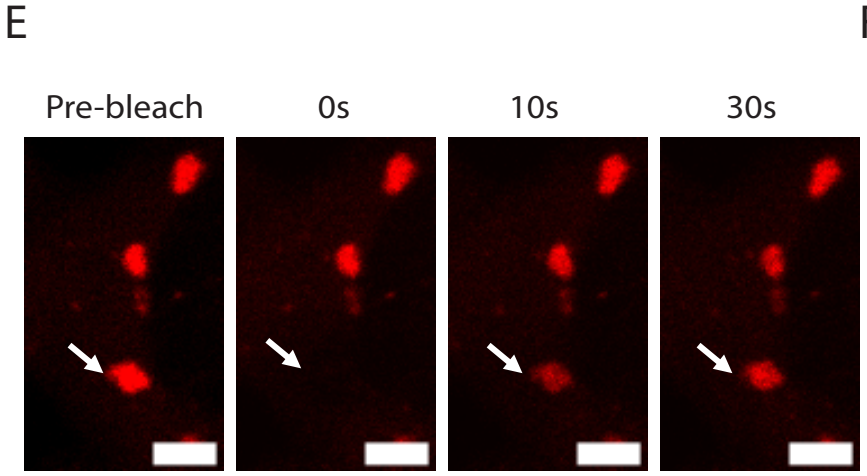
E
Pre-bleach
0s
10s
30s

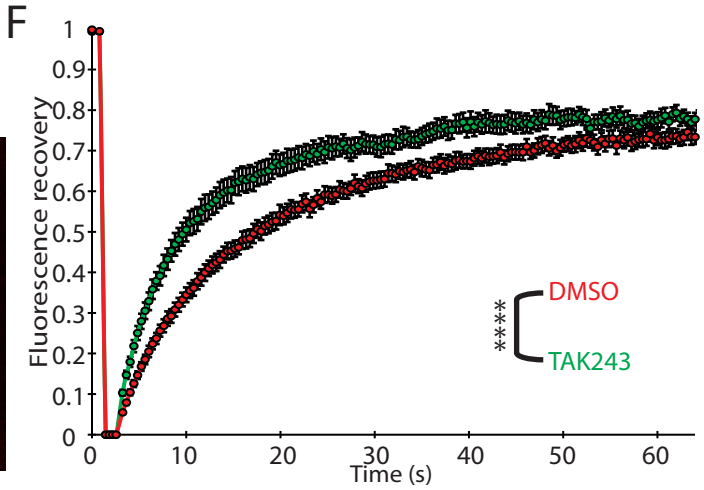
F
Fluorescence recovery
Time (s)
****
DMSO
TAK243

Figure 1. Ubiquitination affects stress granule dynamics and biophysical properties. A. Representative images of U2OS cells overexpressing G3BP1-mCherry with G3BP1/2 KO background, without (DMSO) or with TAK243 (1uM) after 90 min of heat stress at 43 °C (HS) or during recovery at 37 °C for 1h. Scale bar = 20uM. **B.** Quantification of SG number/cell number as a function of time. Data were normalized internally to the time point with maximal SG assembly. ~1000 SG counted per experimental repeat. Nine fields per condition. Data from one experiment out of three experimental repeats (Supplementary fig. 1). Two-way ANOVA with repeated measures. **C.** Quantification of SG number/cell number at 15 min of HS. Average of three experimental repeats shown. Welch's t-test. **D.** Quantification of SG number/cell number at 60 min recovery. Average of three experimental repeats shown. Welch's t-test. **E.** A temporal image series from a FRAP experiment on G3BP1-mCherry U2OS cells under heat stress. Arrow indicates photobleached SG. Scale bar = 5uM. **F.** Quantification of fluorescence recovery after photobleaching in U2OS cells without or with TAK243. Data from one experimental repeat out of three is shown (Supplementary fig. 6). ~20 SGs were counted per experiment. Two-way ANOVA with repeated measures. P value * <0.05; ** <0.01, ****<0.0001.

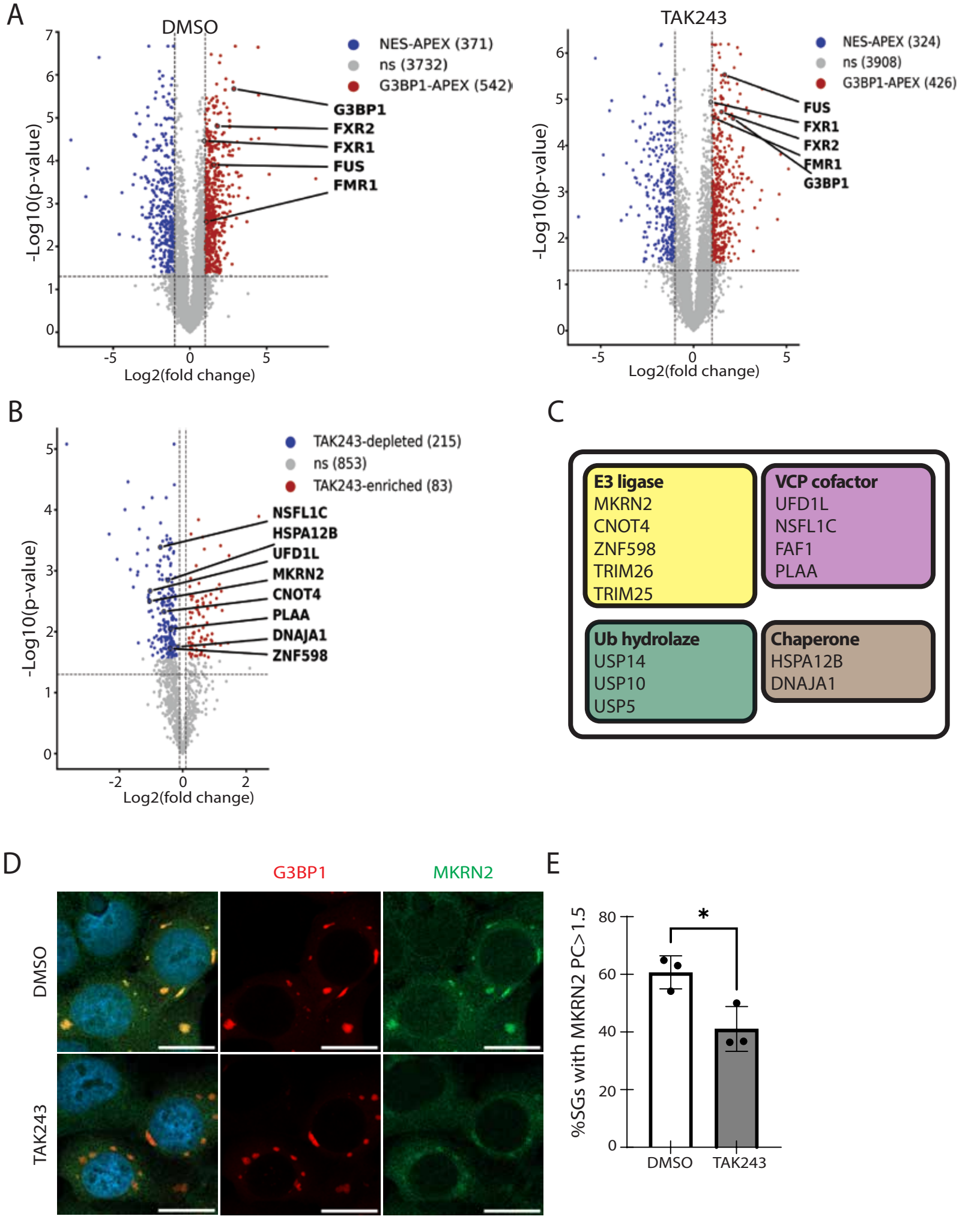
A
DMSO
NES-APEX (371)
ns (3732)
G3BP1-APEX (542)
G3BP1
FXR2
FXR1
FUS
FMR1
-Log10(p-value)
Log2(fold change)
TAK243
NES-APEX (324)
ns (3908)
G3BP1-APEX (426)
FUS
FXR1
FXR2
FMR1
G3BP1
B
TAK243-depleted (215)
ns (853)
TAK243-enriched (83)
NSFL1C
HSPA12B
UFD1L
MKRN2
CNOT4
PLAA
DNAJA1
ZNF598
C
E3 ligase
MKRN2
CNOT4
ZNF598
TRIM26
TRIM25
VCP cofactor
UFD1L
NSFL1C
FAF1
PLAA
Ub hydrolaze
USP14
USP10
USP5
Chaperone
HSPA12B
DNAJA1
D
G3BP1
MKRN2
DMSO
TAK243
E
%SGs with MKRN2 PC>1.5
DMSO
TAK243

Figure 2. Ubiquitination affects stress granule proteomic composition. A. Volcano plot of proteins enriched at the proximity of G3BP1-APEX relative to NES-APEX cytoplasm control (x-axis = Log2 fold change) and statistical significance (y-axis = Log10 p-value). G3BP1/2 KO cells expressing G3BP1-APEX were used to label SG proteins. Induction media contained Biotin phenol, 500uM, and H2O2, 1mM. Labeling activity was quenched 60 seconds after H2O2 addition. **B.** Volcano plot displaying the ubiquitin-dependent enrichment in SG proteins. 83 proteins enriched and 215 proteins depleted from SGs following TAK243 treatment. (x-axis = LogFC; y-axis = log10 p-value). Several E3 ligases, ubiquitin hydrolases, and chaperones (shown in red) are depleted. **C.** Table showing proteostasis factors depleted from SGs upon inhibition of ubiquitination. **D.** Representative images of G3BP1-mCherry cells treated with TAK243 and stained for endogenous MKRN2. **E.** Quantification of the partition coefficient of MKRN2 in SGs in cells treated with DMSO or TAK243. The proportion of SGs with PC>1.5 is shown. Average of three experimental repeats, ~1000 SGs per repeat. Welch's two-sided t-test, p-value * = <0.05; **<0.01, ****<0.0001.

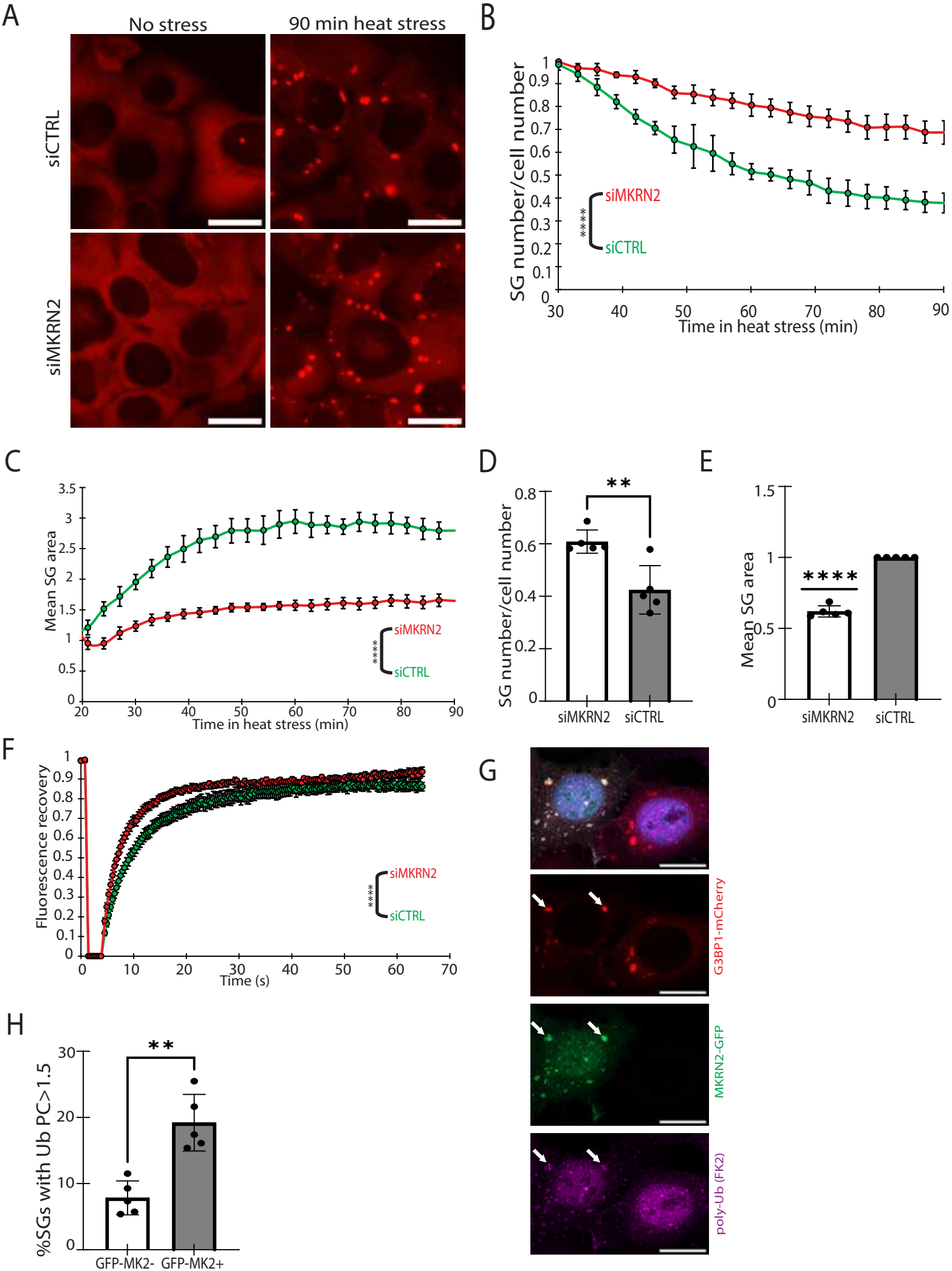
A
No stress
90 min heat stress
siCTRL
siMKRN2
B
SG number/cell number
Time in heat stress (min)
siMKRN2
siCTRL
****
C
Mean SG area
Time in heat stress (min)
siMKRN2
siCTRL
****
D
SG number/cell number
**
siMKRN2
siCTRL
E
Mean SG area
****
siMKRN2
siCTRL
F
Fluorescence recovery
Time (s)
siMKRN2
siCTRL
****
G
G3BP1-mCherry
MKRN2-GFP
poly-Ub (FK2)
H
%SGs with Ub PC>1.5
**
GFP-MK2-
GFP-MK2+

Figure 3. MKRN2 promotes SG assembly and increases SG ubiquitin content. **A.** Representative images of G3BP1-mCherry cells with siMKRN2 vs siCtrl before HS and at 90 min HS at 43 °C. **B.** Quantification of SG number/cell number from 30 min to 90 min HS at 43 °C. Data were normalized internally to the time point with maximal SG assembly. ~1000 SG counted per experiment. Nine fields per condition. Data from one experimental repeat out of five independent experiments. Two-way ANOVA with repeated measures. **C.** Quantification of SG number/cell number at 90 min HS. Average of five experimental repeats shown. Welch's t-test. **D.** Average SG area over the 90 min HS at 43 °C. Data from one experiment out of five experimental repeats. (Supplementary fig. 3). Two-way ANOVA with repeated measures. **E.** Average SG area at 90 min HS at 43 °C. Data were internally normalized to siCtrl. The average of five experimental repeats is shown. One-sample t-test. **F.** Quantification of fluorescence recovery after photobleaching in U2OS cells with either siMKRN2 or siCTRL. Data from one experimental repeat out of three is shown. (Supplementary fig. 6). ~20 SGs were counted per experiment. Two-way ANOVA with repeated measures. **G.** Confocal micrographs of G3BP1-mCherry/MKRN2-GFP U2OS cells stained for poly-ubiquitin (FK2). **H.** FK2 partition coefficient quantification in SGs from either MKRN2-GFP+ vs MKRN2-GFP- cells within the same coverslip. The proportion of SGs with PC>1.5 is shown. Average of 5 experimental repeats shown. >1000 SGs per repeat. p-value * = <0.05; **<0.01, ****<0.0001.

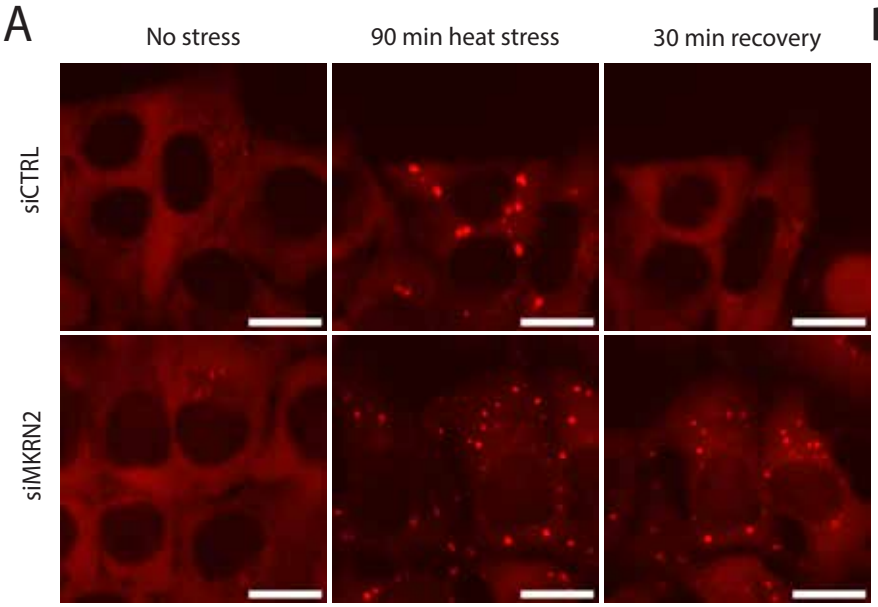
A
No stress
90 min heat stress
30 min recovery
siCTRL
siMKRN2

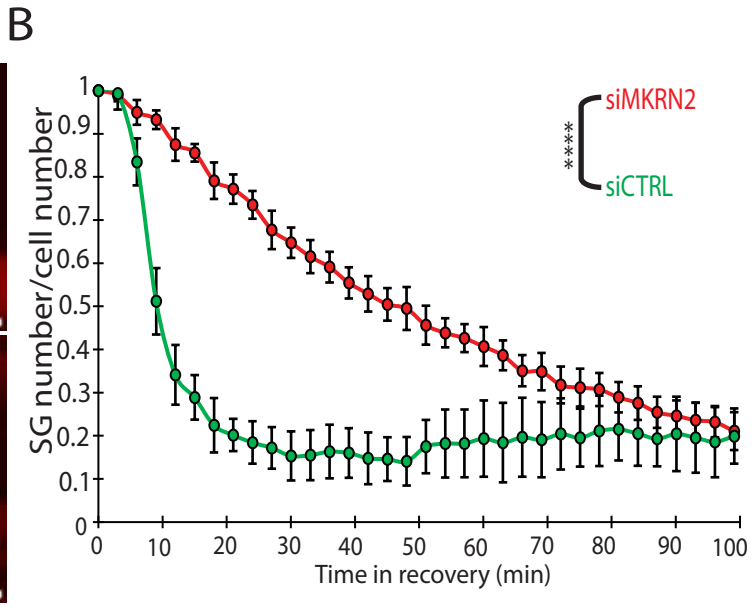
B
SG number/cell number
Time in recovery (min)
siMKRN2
siCTRL
****

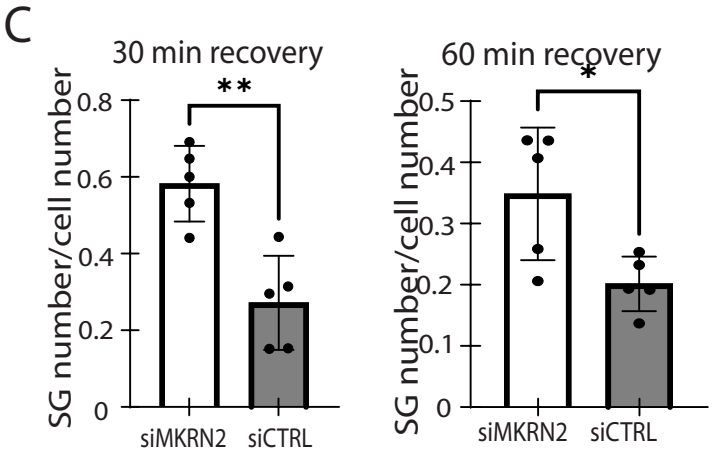
C
30 min recovery
60 min recovery
SG number/cell number
**
*
siMKRN2
siCTRL

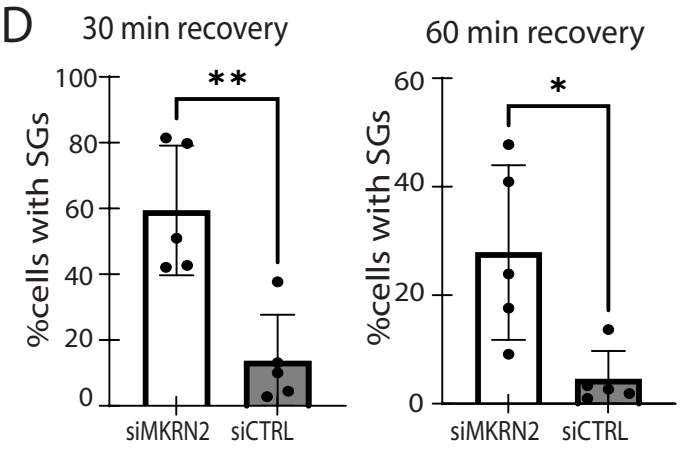
D
30 min recovery
60 min recovery
%cells with SGs
**
*
siMKRN2
siCTRL

Figure 4. MKRN2 promotes SG disassembly. A. Representative images of G3BP1-mCherry cells with siMKRN2 vs siCtrl before HS, at 90 min HS at 43 °C and at 30 min recovery at 37 °C. **B.** Live imaging quantification of SG number/cell number during recovery at 37 °C. Data were internally normalized to 90 min of HS. 9 sites per condition. Data of one experiment out of five experimental repeats. Two-way ANOVA with repeated measures. **C.** Quantification of SG number/cell number at 30 min or 60 min recovery for siMKRN2 vs siCTRL. Average of five experimental repeats shown. Welch's t test. **D.** Quantification of percent cells with SGs at 30 min or 60 min recovery for siMKRN2 vs siCTRL. Average of five experimental repeats shown. Welch's t-test. p-value * = <0.05; **<0.01, ****<0.0001.

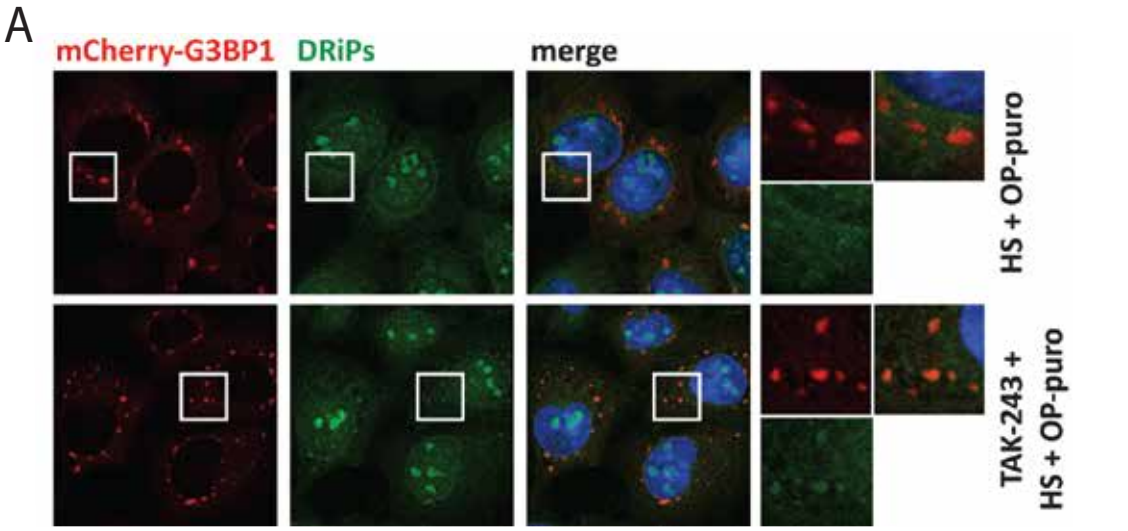
A
mCherry-G3BP1
DRiPs
merge
HS + OP-puro
TAK-243 +
HS + OP-puro

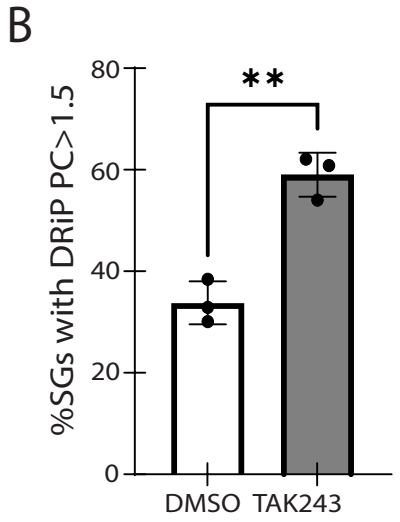
B
%SGs with DRiP PC>1.5
80
60
40
20
0
**
DMSO
TAK243

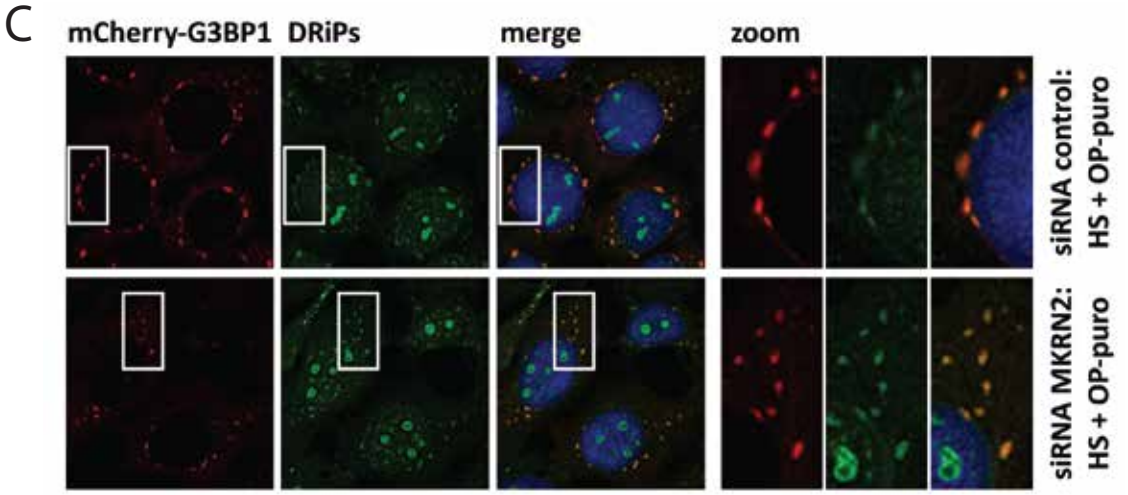
C
mCherry-G3BP1
DRiPs
merge
zoom
siRNA control:
HS + OP-puro
siRNA MKRN2:
HS + OP-puro

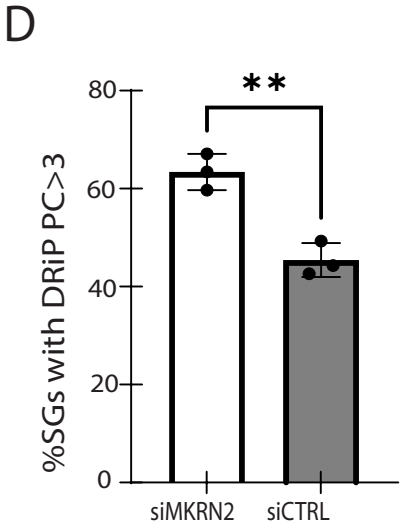
D
%SGs with DRiP PC>3
80
60
40
20
0
**
siMKRN2
siCTRL

Figure 5. Ubiquitination is required for preventing DRiP accumulation in SGs. A. Representative images of DMSO vs TAK243 G3BP1-mCherry U2OS cells treated with 25 μM OP-puro to label DRiPs and heat-stressed at 43 °C for 60 min to induce SGs. **B.** Quantification of the partition coefficient of DRiPs in SGs from cells treated with either DMSO or TAK243. The proportion of SGs with PC>1.5 is shown. Welch's t-test. **C.** Representative images of siMKRN2 vs siCTRL G3BP1-mCherry U2OS cells treated with 25 μM OP-puro to label DRiPs and heat-stressed at 43 °C. **D.** Quantification of the partition coefficient of DRiPs in SGs from cells treated with either siMKRN2 or siCTRL. The proportion of SGs with PC>1.5 is shown. Welch's t-test. **<0.01

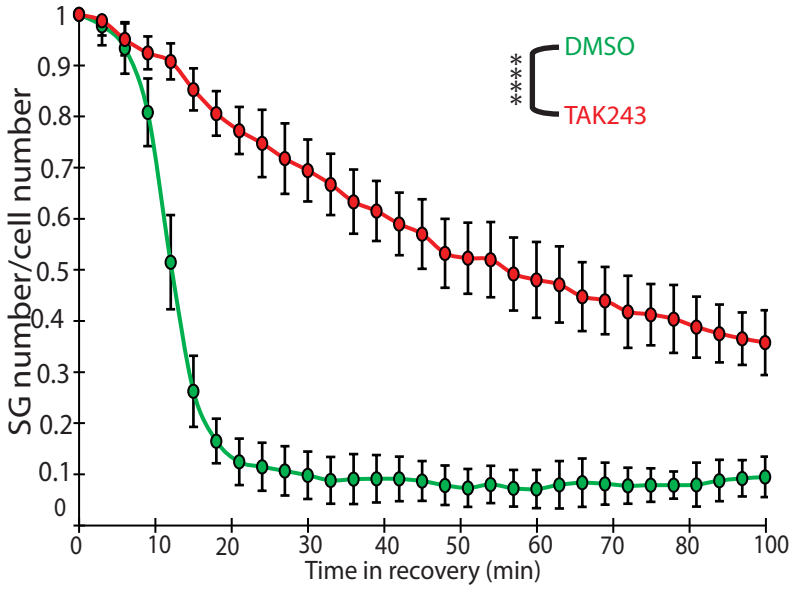
SG number/cell number
Time in recovery (min)
DMSO
TAK243
****

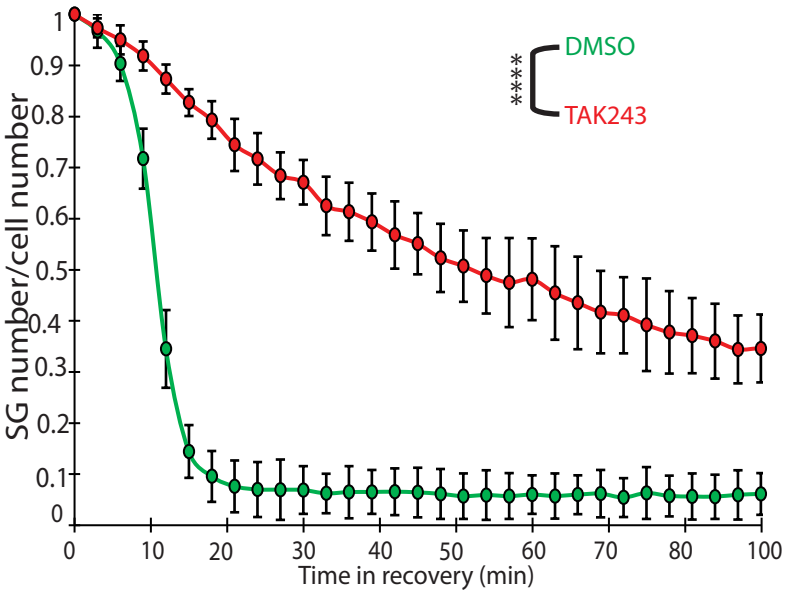
SG number/cell number
Time in recovery (min)
DMSO
TAK243
****

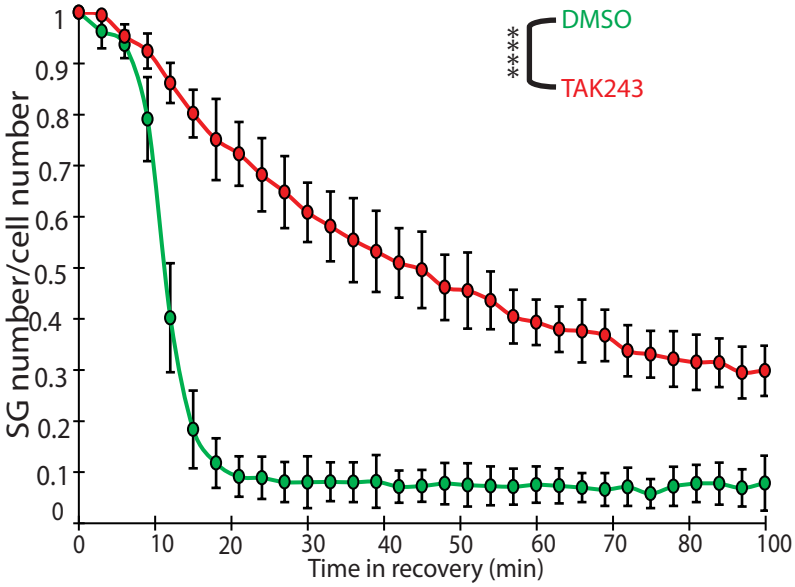
SG number/cell number
Time in recovery (min)
DMSO
TAK243
****

Supplementary figure 1. SG disassembly live imaging repeats with TAK243. Live imaging quantification of SG number/cell number during recovery at 37°C. Data were internally normalized to 90 min of HS. 9 sites per condition. Three experimental repeats shown. Two-way ANOVA with repeated measures. ****<0.0001.

A

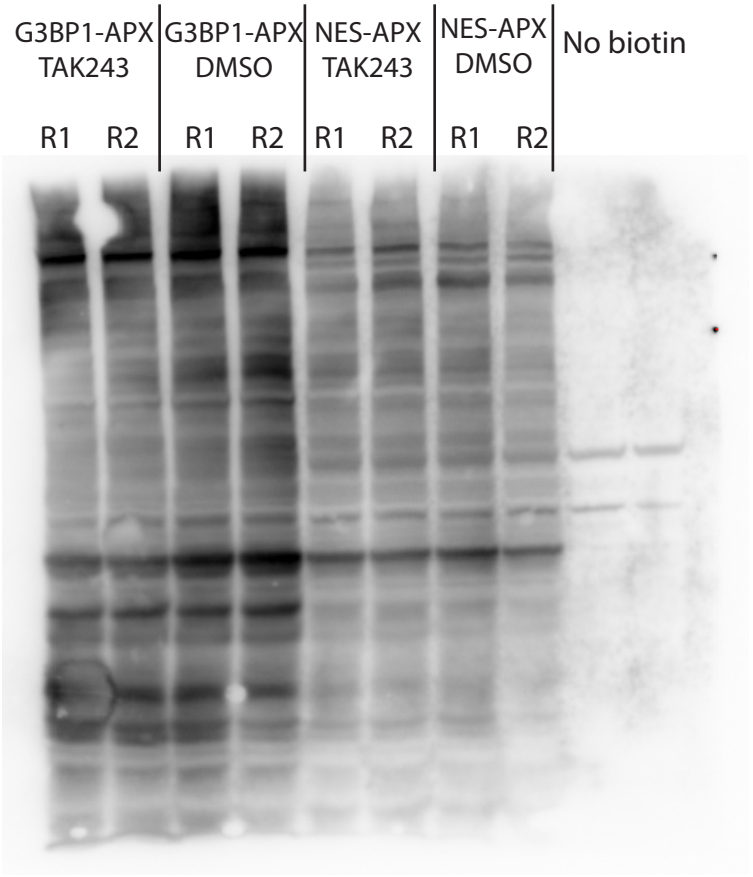
G3BP1-APX TAK243
G3BP1-APX DMSO
NES-APX TAK243
NES-APX DMSO
No biotin
R1 R2 R1 R2 R1 R2 R1 R2

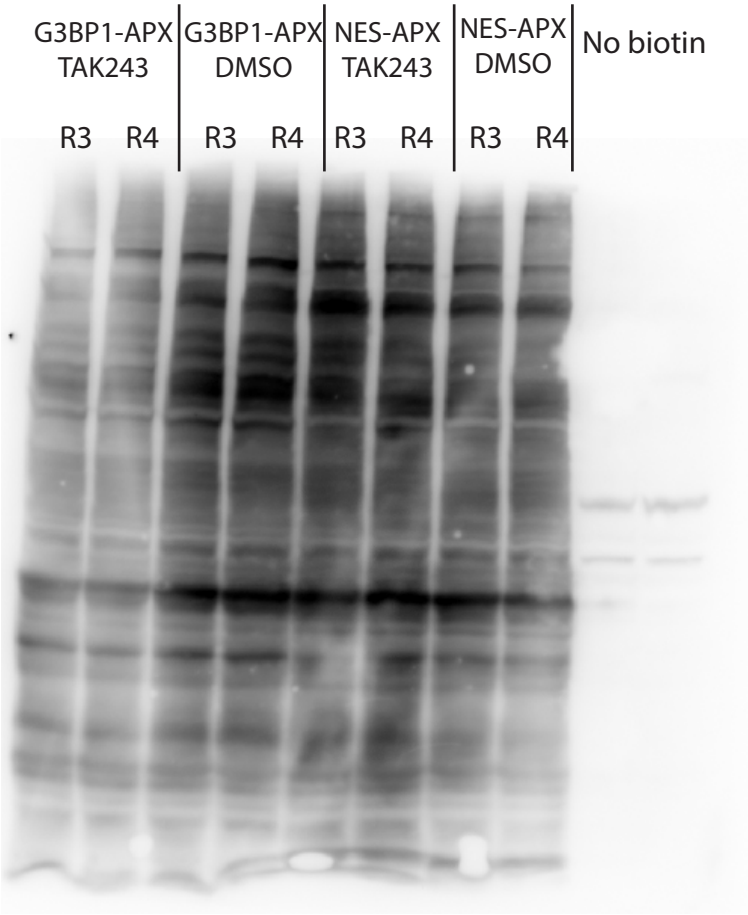
G3BP1-APX TAK243
G3BP1-APX DMSO
NES-APX TAK243
NES-APX DMSO
No biotin
R3 R4 R3 R4 R3 R4 R3 R4

B

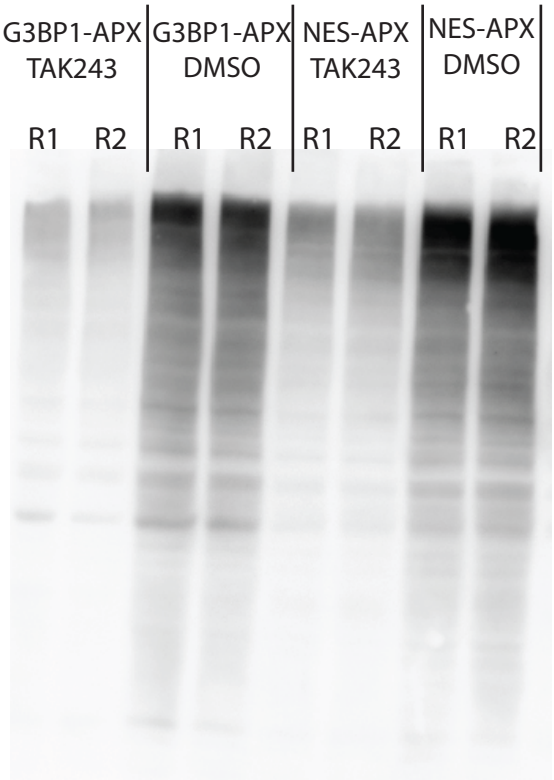
G3BP1-APX TAK243
G3BP1-APX DMSO
NES-APX TAK243
NES-APX DMSO
R1 R2 R1 R2 R1 R2 R1 R2

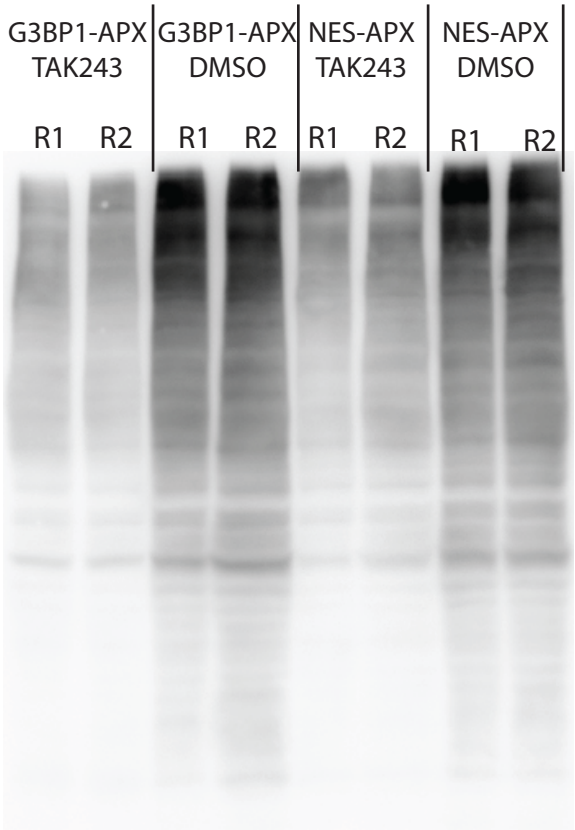
G3BP1-APX TAK243
G3BP1-APX DMSO
NES-APX TAK243
NES-APX DMSO
R1 R2 R1 R2 R1 R2 R1 R2

Supplementary figure 2. APEX samples. A. Anti-Biotin Western blot for samples used in APEX proteomics experiment. **B.** Ant-ubiquitin (FK2) Western blot for samples used in APEX proteomics experiment.

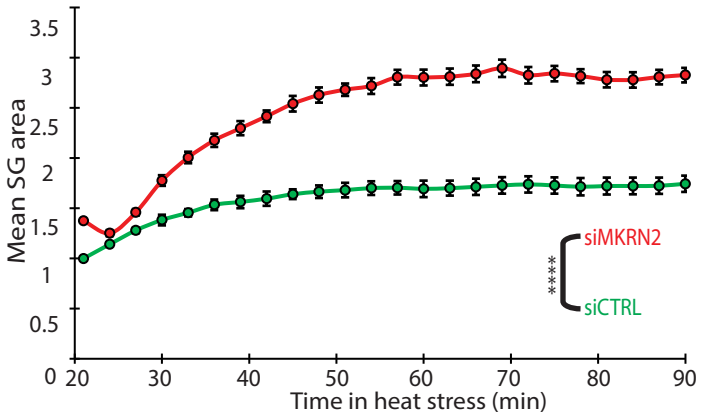
Mean SG area
Time in heat stress (min)
siMKRN2
siCTRL
****

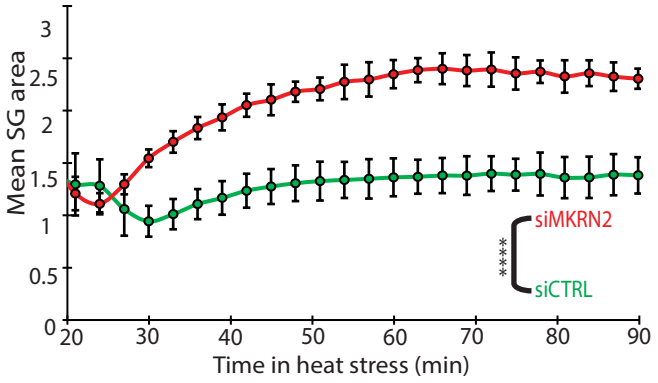
Mean SG area
Time in heat stress (min)
siMKRN2
siCTRL
****

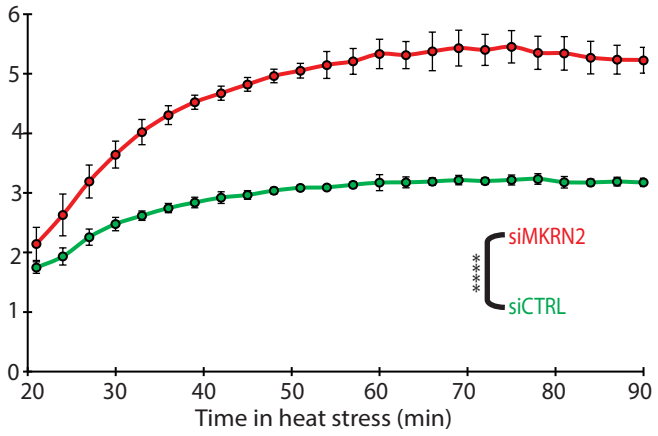
Time in heat stress (min)
siMKRN2
siCTRL
****

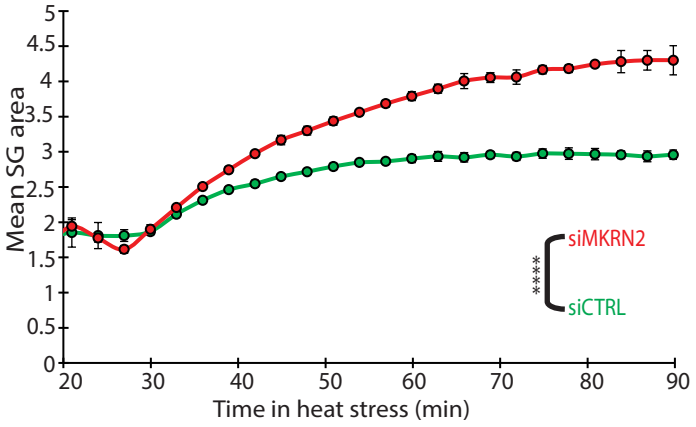
Mean SG area
Time in heat stress (min)
siMKRN2
siCTRL
****

Supplementary figure 3: SG assembly live imaging repeats with MKRN2 KD. Live imaging quantification of SG area during HS at 43°C. 9-12 sites per condition. Four experimental repeats shown (fifth repeat shown in Fig. 3C). Two-way ANOVA with repeated measures. ****<0.0001.

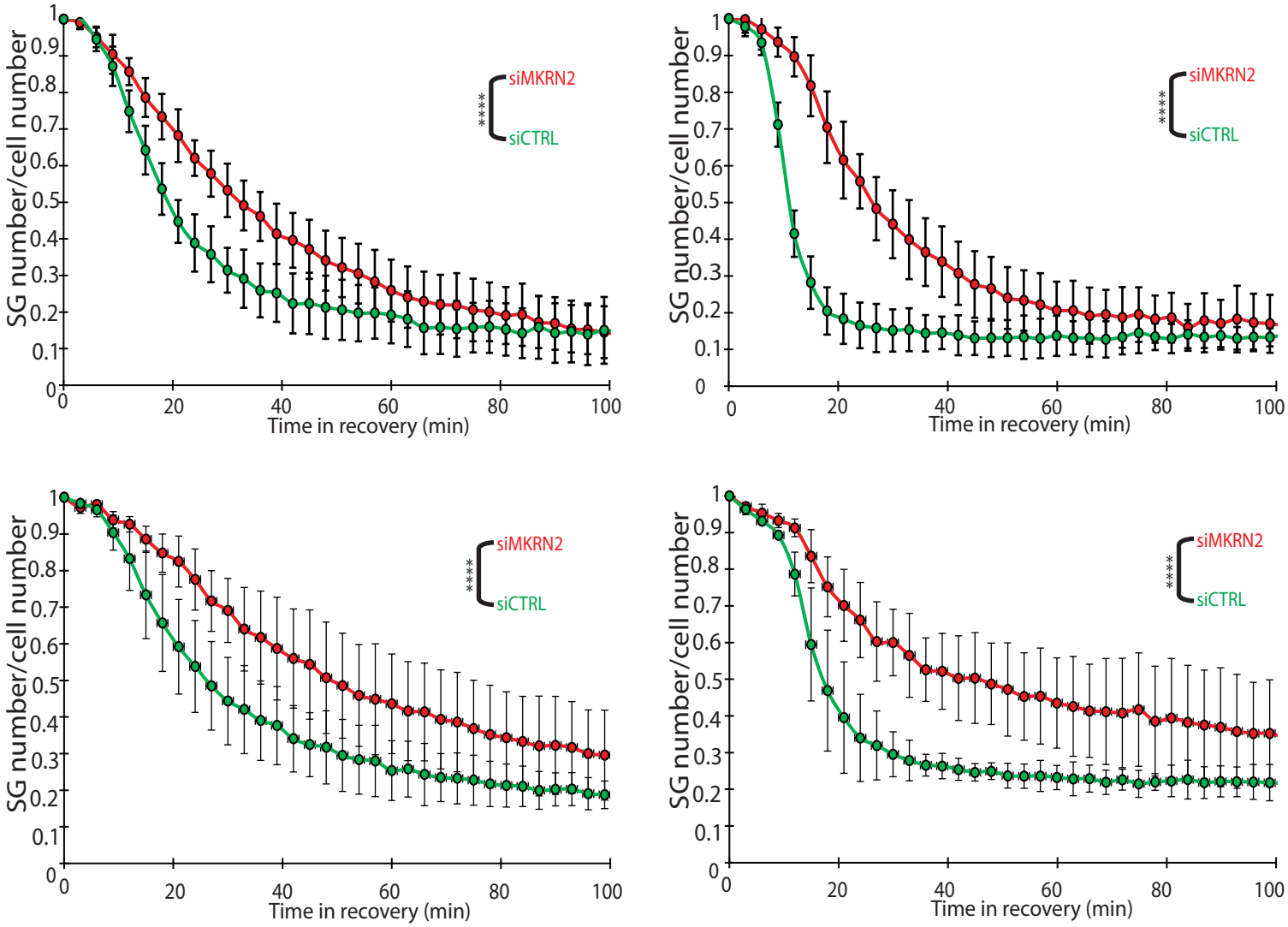
SG number/cell number
Time in recovery (min)
siMKRN2
siCTRL
****
0
0.1
0.2
0.3
0.4
0.5
0.6
0.7
0.8
0.9
1
0
20
40
60
80
100

Supplementary figure 4. SG disassembly live imaging repeats with MKRN2 KD. Live imaging quantification of SG number/cell number during recovery at 37°C. Data were internally normalized to 90 min of HS. 9-12 sites per condition. Four experimental repeats shown (fifth repeat shown in Fig. 4B). Two-way ANOVA with repeated measures. ****<0.0001.

A

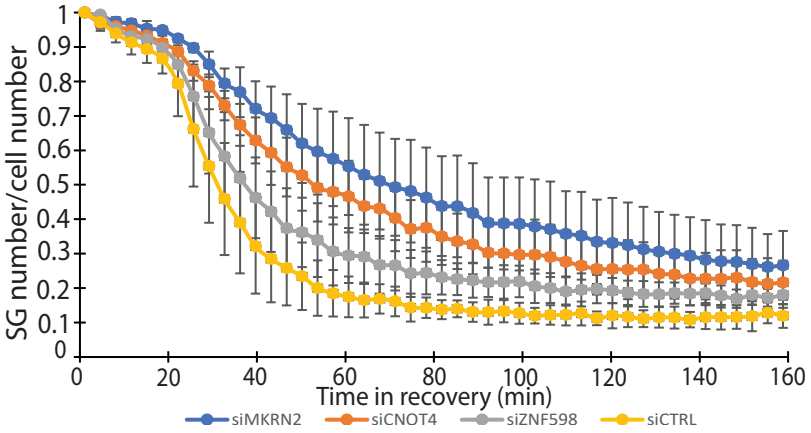
SG number/cell number
1
0.9
0.8
0.7
0.6
0.5
0.4
0.3
0.2
0.1
0
0
20
40
60
80
100
120
140
160
Time in recovery (min)
siMKRN2
siCNOT4
siZNF598
siCTRL

B

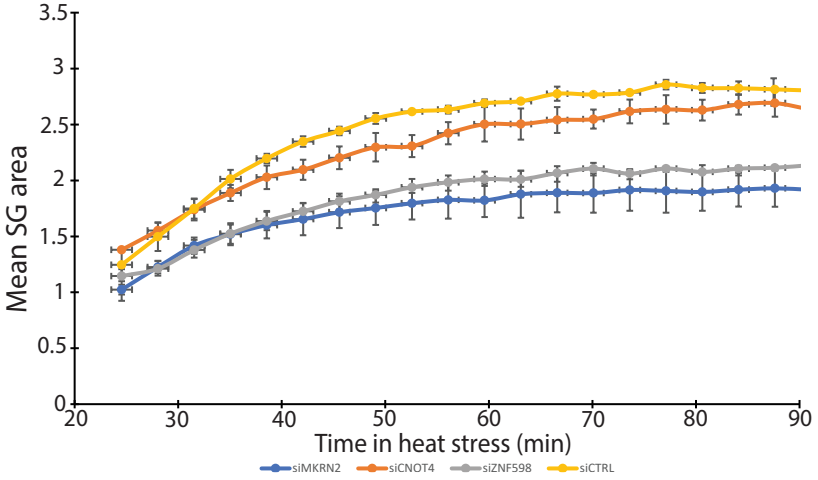
Mean SG area
3.5
3
2.5
2
1.5
1
0.5
0
20
30
40
50
60
70
80
90
Time in heat stress (min)
siMKRN2
siCNOT4
siZNF598
siCTRL

Supplementary figure 5. Live imaging with MKRN2, ZNF598 and CNOT4. A. SG number/cell number during stress recovery (normalized to 90 min HS). **B.** Average SG area over time in HS.

A

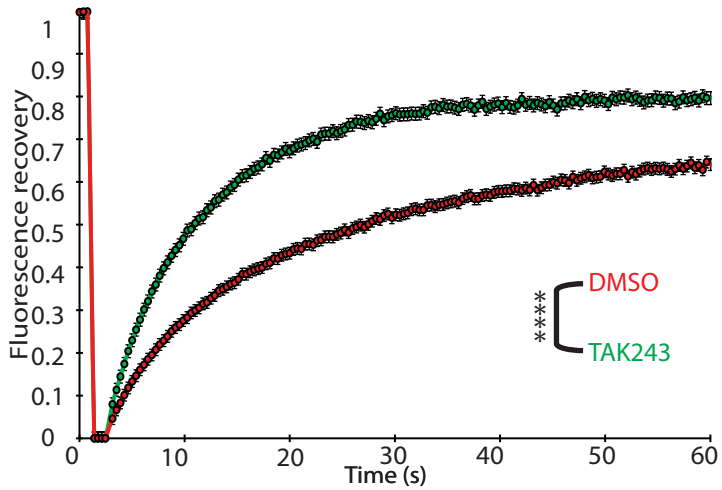
Fluorescence recovery
Time (s)
DMSO
TAK243
****

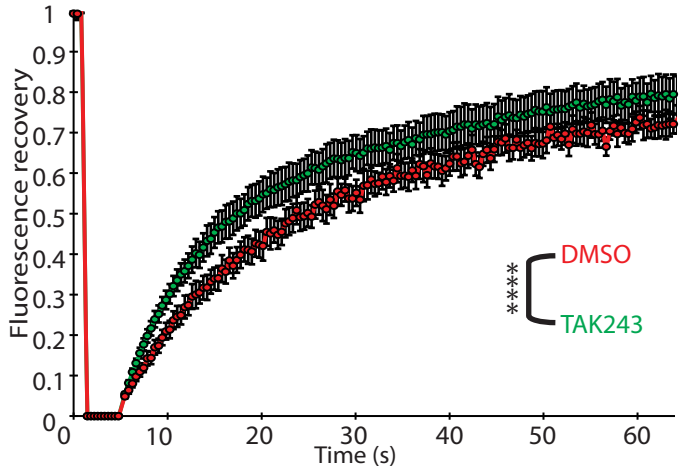
Fluorescence recovery
Time (s)
DMSO
TAK243
****

B

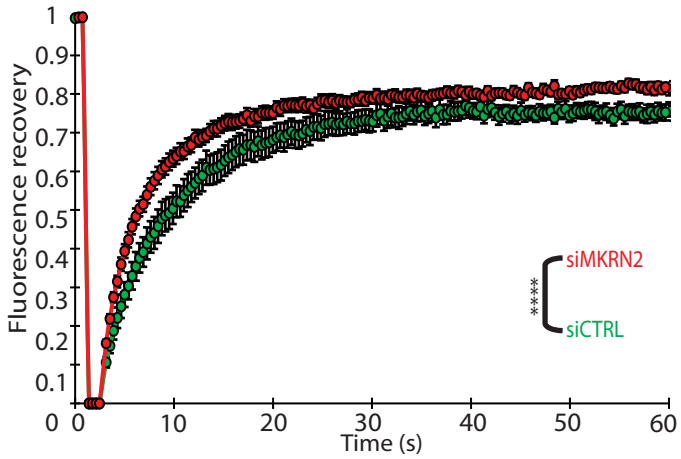
Fluorescence recovery
Time (s)
siMKRN2
siCTRL
****

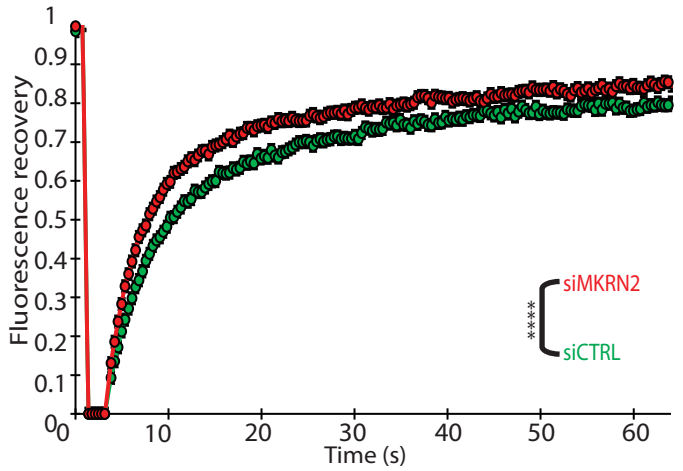
Fluorescence recovery
Time (s)
siMKRN2
siCTRL
****

Supplementary figure 6: FRAP repeats. A. Quantification of fluorescence recovery after photobleaching in TAK243 vs control cells. Two experimental repats shown (third repeat in Fig. 1F). ~20 SGs per repeat. **B.** Quantification of fluorescence recovery after photobleaching in TAK243 vs control cells. Two experimental repats shown (third repeat in Fig. 3F). ~20 SGs per repeat. Two way ANOVA with repeated measures. ****<0.0001.